Mathematical Medicine and Biology Page 1 of 26
doi:10.1093/imammb/dqnxxx

Simple Model of Atherosclerosis in Cylindrical Arteries: Impact of Anisotropic Growth on Glagov Remodeling

NAVID MOHAMMAD MIRZAEI
Dept. of Mathematical Sciences, University of Delaware, Newark, DE, 19716, USA.

PAK-WING FOK
Dept. of Mathematical Sciences, University of Delaware, Newark, DE, 19716, USA.

In 1987, Seymour Glagov observed that arteries went through a two-stage remodeling process as a result of plaque growth: first, a compensatory phase where the lumen area remains approximately constant and second, an encroachment phase where the lumen area decreases over time. In this paper we investigate the effect of growth anisotropy on Glagov remodeling in five different cases: pure radial, pure circumferential, pure axial, isotropic and general anisotropic growth where the elements of the growth tensor are chosen to minimize the total energy. We suggest that the nature of anisotropy is inclined towards the growth direction that requires the least amount of energy. Our framework is the theory of morphoelasticity on an axisymmetric arterial domain. For each case we explore their specific effect on the Glagov curves. For the latter two cases we also provide the changes in collagen fiber orientation and length in the intimate, media and adventitia. In addition, we compare the total energy produced by growth in radial, circumferential and axial direction and deduce that using a radially dominant anisotropic growth leads to lower strain energy than isotropic growth.

Keywords: Glagov remodeling, morphoelasticity, anisotropic growth, arterial biomechanics, atherosclerosis, intimal thickening.

1. Introduction

Despite the recent advances in preventive methods, cardiovascular disease (CVD) is still the global leading cause of death. It accounted for about 841,000 deaths (635,260 cardiac) in 2016 with the annual total cost of $351.2 billion in 2014-2015 in the United States (Benjamin et al. (2019)).

Atherosclerosis is a cardiovascular disease which can cause the narrowing of blood vessels therefore reducing the blood flow. It can lead to life-threatening problems including heart attack and stroke. A healthy artery wall consists of three layers: intima, media and adventitia. Intima is the innermost layer and the media and adventitia are the middle and outermost layers respectively. It is known that the intima is the main region for plaque buildup and consequently atherosclerotic lesions (Virmani et al. (2008)).

According to Virmani et al. (2008), the evolution of vascular disease involves a combination of endothelial dysfunction, extensive lipid deposition in the intima, an exacerbated immune response, proliferation of vascular smooth muscle cells and remodeling, resulting in the formation of an atherosclerotic plaque. High risk atherosclerotic plaques (vulnerable plaques) have a large lipid-rich necrotic core with an overlying thin fibrous cap infiltrated by inflammatory cells and diffuse calcification. These plaques are more susceptible to rupture. Plaque rupture occurs in 1% to 6% of patients and accounts for 15% of in-hospital deaths (Antman (2007)).

Low shear stress plays an essential role in atherosclerosis (Libby et al. (2002), Mundi et al. (2017), Channon (2006)). Healthy endothelial cells produce a certain amount of Nitric Oxide (NO) which is a vasodilator. Decrease in laminar shear stress reduces the production of this chemical which leads to endothelial dysfunction. This increases the permeability of the endothelium to low density lipoproteins (LDL) as well as the production of vascular cell adhesion molecule-1 (VCAM-1). These molecules start an inflammatory process by binding with intracellular adhesion molecule-1 (ICAM-1) on the surface of leukocytes present in the blood stream. Attached to the endothelium, these leukocytes penetrate the vessel wall in response to chemoattractant MCP-1 present in the intima. Once inside, macrophage colony stimulating factor (M-CSF) causes them to turn into macrophages. LDLs absorbed by the intima go through oxidation and turn into oxidized LDLs. Macrophages consume these oxidized LDLs and release more MCP-1, turning into foam cells. Smooth muscle cells (SMCs) can also migrate into the plaque from the underlying media. The death of SMCs, foam cells and macrophages all contribute to a necrotic core, one of the defining characteristics of a vulnerable plaque (Libby et al. (2002), Virmani et al. (2008)).

Investigating the mechanical properties of the blood vessels is an essential step towards understanding cardiovascular diseases. Taber & Humphrey (2001) investigated the stress-modulated growth and residual stress of the arteries using the concept of opening angles. In their research they considered the artery as a single-layered domain and speculated that the opening angles as a measurement for residual stresses depend strongly on the heterogeneity of the material properties. The intima was considered to be mechanically insignificant. Due to its thinness, the other two layers were often considered as the main "load bearing" layers (Von Maltzahn et al. (1981), Demiray & Vito (1991)). The significance of the intima was shown by Holzapfel et al. (2005). They determined the mechanical properties of coronary artery layers with nonatherosclerotic intimal thickening. In their study, they experimented on thirteen hearts, from 3 women and 10 men which were harvested within 24 hours of death. Then they created coronary artery cross sections and cut them along the axial direction to obtain flat rectangular sheets. Thereafter, by exposing the sheets to tensile stresses, they were able to come up with layer-specific mechanical parameters later used in their strain energy function. This function is able to capture the stiffening effect of collagen fibers that exist in each layer. It also turned out that the stiffness parameters for the intima were significantly larger than the other two layers.

There are many studies that try to understand the cell and chemical dynamics of intimal thickening and atherosclerosis using reaction-diffusion type models. One can find a comprehensive example in Hao & Friedman (2014). They have most of the key players including a velocity field which is the result of movement of macrophages, T-cells and smooth muscle cells into the intima. This procedure promotes intimal thickening. Their model however, does not consider the mechanical properties of the intima and neglects the other two layers of the vessel wall. For this reason it qualifies as a reaction-diffusion type model. Chalmers et al. (2015) use differential equations to purely explore the dynamics of early atherosclerosis. Their model considers the concentration of LDLs, chemoattractants, embryonic stem (ES) cytokines, macrophages and foam cells. All of their simulations are done in one dimension and their result provides qualitative and quantitative insight into the effect of LDL penetration in the inflammatory response. In Chalmers et al. (2017), the authors investigate the effect of High density Lipoproteins (HDL) in plaque regression. El Khatib et al. (2007) suggest that inflammation propagates in the intima as a reaction diffusion wave. They conclude that in the case of intermediate LDL concentrations there are two stable equilibria: one corresponding to the disease free state and the other one to the inflammatory state while the traveling wave connects these two states.

Glagov et al. (1987) studied sections from the left main coronary artery in 136 hearts obtained at autopsy. He found that arterial remodeling happens in two stages: compensation and encroachment.

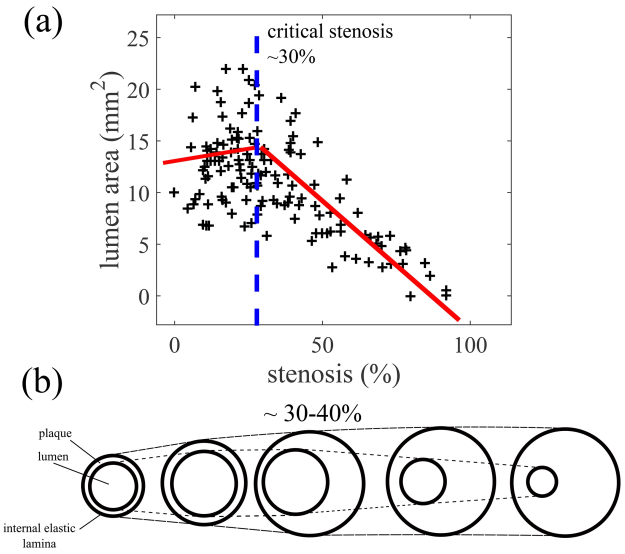

FIG. 1: Remodeling behavior depends on whether stenosis is less than or greater than 30%. With the same data, the authors were also able to fit a piecewise linear curve with a jump in derivative at about 40% (not shown). In this case, the curve gently decreased when the stenosis was $< 40\%$ and rapidly decreased when the stenosis was $> 40\%$. (b) In Glagov remodeling, initially, the lumen area increases slightly while the internal elastic lamina (IEL) increases in area. After the plaque reaches about 40% of the IEL area, the luminal area starts to decrease.

During the compensation phase the area enclosed by the endothelial wall (lumen area) increases. This compensation will continue until the lesion occupies about 40% of the area enclosed by the internal elastic lamina. In other words, the vessel compensates for plaque growth until it reaches about 40% stenosis where

$$\text{Stenosis} = \frac{\text{Intima Area}}{\text{Intima Area} + \text{Lumen Area}} \tag{1.1}$$

and then the decrease in of the lumen area (encroachment) starts (Figure 1). Understanding this phenomenon is of great importance. Since coronary angiography can only visualize the lumen the extent of the plaque burden in the arterial wall might be underestimated during the compensation phase. Therefore, understanding this property of blood vessels is crucial for devising new methods for determining the severity of arterial diseases such as atherosclerosis. This phenomenon has been the subject of biological and mathematical studies ever since (Korshunov & Berk (2004), Mohiaddin et al. (2004), Korshunov et al. (2007) and Fok (2016)). Fok (2016) explores the growth in a 2D annulus subject to a uniform isotropic growth tensor. Although these assumptions are not realistic the results seem to follow the general characteristics of Glagov remodeling.

In this paper we focus on a three dimensional axisymmetric vessel wall with 3 layers. We assume that the plaque in our problem is homogeneous. This means we neglect the heterogeneities caused in the plaque such as cholesterol crystals, calcium, cell debris, foam cells that might affect the plaque growth. We consider a static blood pressure of 120 mmHg as the average of systolic and diastolic pressures. We neglect long term changes in the blood pressure so that we can focus on understanding how growth affects remodeling and the Glagov curve. We use a finite element method based on morphoelasticity. We utilize the layer specific strain energy function proposed in Holzapfel et al. (2005) to account for

the stiffening effect of the collagen fibers. All of our numerical simulations are carried out in a FEniCS framework (Langtangen et al. (2016)). Although there are various studies involving the artery growth in two dimensions, we will see that growth in three dimensions produces interesting results. We provide results that show for example, anisotropic growth is energetically more favorable than isotropic growth and at the same time results in a greater stenosis. In addition, anisotropic treatment of the problem results in more stenosis that is more in line with what Glagov observed in a more energetically favorable manner (Glagov et al. (1987)).

This paper is laid out in the following way. In section 2 we discuss the morphoelastic modeling of our problem. In section 3 we provide our results and finally we summarize our conclusions in section 4.

2. The variational formulation

Morphoelasticity is the underlying assumption for our simulations. It interprets the deformation in hyperelastic materials as a pure growth accompanied by an elastic response (Goriely & Amar (2007), Rodriguez et al. (1994)). In other words, we can decompose the deformation gradient into a growth tensor $\mathbf{G}$ (which we prescribe) and an elastic tensor $\mathbf{F}_e$ (which has to be found):

$$\mathbf{F} = \mathbf{F}_e\mathbf{G}. \tag{2.1}$$

As mentioned before we consider the artery as a three layered growing domain. This growth is a volumetric growth that occurs only inside the intima and can also be accompanied by surface loads. Corresponding to each of the tensors in (2.1) we have

$$J = \det(\mathbf{F}), \tag{2.2}$$
$$J_e = \det(\mathbf{F}_e), \tag{2.3}$$
$$J_g = \det(\mathbf{G}). \tag{2.4}$$

Deformation and growth of the artery lead to a change in the strain energy W. This strain energy is the sum of energy stored due to the isotropic (Ψ_{iso}) and the anisotropic (Ψ_{aniso}) changes in each of the layers (**?**):

$$W_i = \Psi^i_{\text{iso}} + \Psi^i_{\text{aniso}}$$

$$\Psi^i_{\text{iso}} = \frac{\mu_i}{2}(I_1 - 3) + \frac{\nu}{1-2\nu}\mu_i(J_e - 1)^2 - \mu_i \ln J_e \tag{2.5}$$

$$\Psi^i_{\text{aniso}} = \frac{\eta_i}{\beta_i}\left\{e^{\beta_i\left[\rho_i(I_4-1)^2_+ + (1-\rho_i)(I_1-3)^2\right]} - 1\right\} \tag{2.6}$$

where $i = 1,2,3$ corresponds to intima, media and adventitia; μ_i, η_i are stress-like parameters; and β_i, ρ_i are dimensionless. Due to the high content of water in each layer we consider them as nearly incompressible materials and therefore we take the Poisson ratio ν to be close to 0.5 in all the layers. This will guarantee that the the second term on the right hand side of equation (2.5) will be significant when minimizing the total strain energy: the minimization will strongly penalize $J_e \neq 1$ which enforces the near incompressibility of the material. Also define

$$I_1 = \text{Tr}(\mathbf{C}_e) = \text{Tr}(\mathbf{F}_e^T\mathbf{F}_e) \tag{2.7}$$
$$I_4 = \mathbf{b}(R,Z)^T\mathbf{C}_e\mathbf{b}(R,Z) \tag{2.8}$$

where $\mathbf{C}_e = \mathbf{F}_e^T \mathbf{F}_e$ is the right Cauchy-Green tensor and I_1 is its first invariant. To incorporate the direction for which the collagen fibers are aligned in each of the layers we use $\mathbf{b}(R,Z)$ which is a unit vector. Because of the crimped structure of collagen it is regarded as not being able to support compressive stresses (Holzapfel et al. (2000)). The role of the collagen fibers is included in the $(I_4-1)_+^2$ term in equation (2.6) which will be triggered only if $I_4 > 1$:

$$(I_4-1)_+^2 = \begin{cases} (I_4-1)^2 & \text{if } I_4 > 1 \\ 0 & \text{if } I_4 \leqslant 1 \end{cases}$$

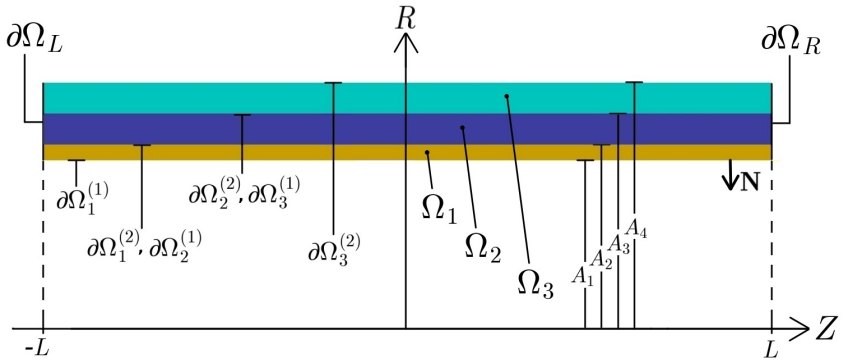

(a)

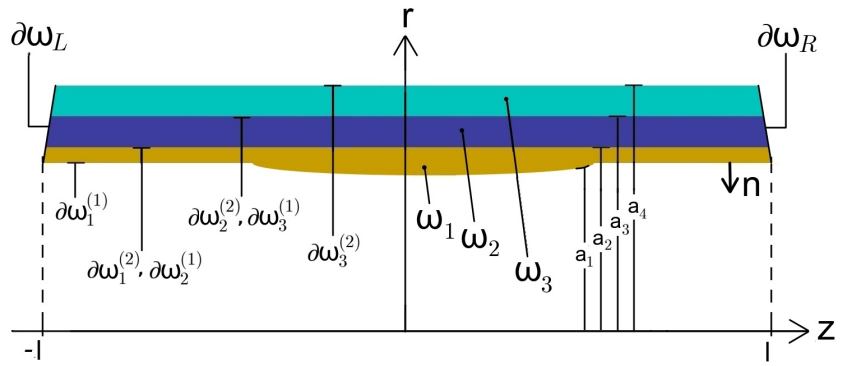

(b)

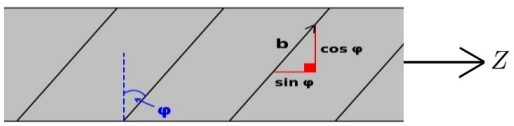

(c)

FIG. 2: (a) Mathematical reference domain with subdomains and boundary labels. (b) Mathematical deformed domain with subdomains and boundary labels. We use lower case letters for the deformed domain. (c) Plan view of the artery and the orientation of representative fibers. Vector **b** is defined for each layer by (2.28) and the values of φ for each layer are given in Table 1.

We are interested in finding a solution to the following boundary value problem

$$\nabla \cdot \boldsymbol{\sigma} = -\hat{\mathbf{f}}, \qquad \text{on } \omega \tag{2.9}$$
$$\boldsymbol{\sigma}\mathbf{n} = -p\mathbf{n}, \qquad \text{on } \partial\omega_1^{(1)} \tag{2.10}$$
$$\boldsymbol{\sigma}\mathbf{n} = 0, \qquad \text{on } \partial\omega_3^{(2)} \tag{2.11}$$
$$\boldsymbol{\sigma}\mathbf{n}|_{\partial\omega_1^{(2)}} + \boldsymbol{\sigma}\mathbf{n}|_{\partial\omega_2^{(1)}} = 0 \tag{2.12}$$
$$\boldsymbol{\sigma}\mathbf{n}|_{\partial\omega_2^{(2)}} + \boldsymbol{\sigma}\mathbf{n}|_{\partial\omega_3^{(1)}} = 0 \tag{2.13}$$

Where the tensor $\boldsymbol{\sigma}$ is the Cauchy stress tensor, $\hat{\mathbf{f}}$ is the body force, $\omega = \bigcup_{i=1}^{3} \omega_i$ for $i = 1,2,3$ is the three layered domain after deformation and $\partial\omega_i^{(1)}$ is the inner boundary and $\partial\omega_i^{(2)}$ is the outer boundary of the i-th layer after the deformation. We consider p to be the only boundary load which in our case is the blood pressure. We denote the outward unit normal vector to the deformed boundary by $\mathbf{n}$. Given that stenotic coronary arteries generally experience very little axial pre-stretch (Gasser & Holzapfel (2007), Sanyal & Han (2015)) we add two traction free boundary conditions for the end surfaces

$$\boldsymbol{\sigma}\mathbf{n} = 0, \qquad \text{on } \partial\omega_L \tag{2.14}$$
$$\boldsymbol{\sigma}\mathbf{n} = 0, \qquad \text{on } \partial\omega_R \tag{2.15}$$

Even though, (2.9)-(2.15) seem like a typical boundary value problem, due to the convenience of working with the reference domain, Ω we prefer to use a system that utilizes $\partial\Omega$ for its boundary condition rather than $\partial\omega$, see Figure 2(a). Therefore, by applying Nanson's pull back formula (Holzapfel (2000)) and using the first Piola-Kirchoff stress tensor, (2.9)-(2.15) turn into

$$\nabla \cdot \mathbf{T} = -\mathbf{f}, \qquad \text{on } \Omega_1,\, \Omega_2,\, \Omega_3 \tag{2.16}$$
$$\mathbf{T}\mathbf{N} = -pJ\mathbf{F}^{-T}\mathbf{N}, \qquad \text{on } \partial\Omega_1^{(1)} \tag{2.17}$$
$$\mathbf{T}\mathbf{N} = 0, \qquad \text{on } \partial\Omega_3^{(2)} \tag{2.18}$$
$$\mathbf{T}\mathbf{N}|_{\partial\Omega_1^{(2)}} + \mathbf{T}\mathbf{N}|_{\partial\Omega_2^{(1)}} = 0 \tag{2.19}$$
$$\mathbf{T}\mathbf{N}|_{\partial\Omega_2^{(2)}} + \mathbf{T}\mathbf{N}|_{\partial\Omega_3^{(1)}} = 0 \tag{2.20}$$
$$\mathbf{T}\mathbf{N} = 0, \qquad \text{on } \partial\Omega_L \tag{2.21}$$
$$\mathbf{T}\mathbf{N} = 0, \qquad \text{on } \partial\Omega_R \tag{2.22}$$

where the first Piola-Kirchoff stress is

$$\mathbf{T} = J_g \frac{\partial W}{\partial \mathbf{F}_e}\mathbf{G}^{-T} \tag{2.23}$$

(Amar & Goriely (2005), Yin et al. (2019)). Also $\mathbf{f}(X,Y,Z) = J\hat{\mathbf{f}}$ (Gurtin (1981)) and $\mathbf{N}$ is the outward unit normal vector to the reference boundary, see Figure 2(a). Boundary conditions (2.14)-(2.15) or (2.21)-(2.22) can be recast in terms of displacement. This may be the more convenient type of condition to use if we have information about the artery's axial prestretch. For solving this problem we use a weak form that is equivalent to (2.16)-(2.22).

2.1 *Weak formulation in cylindrical coordinates*

We consider an axisymmetric cylindrical domain Ω with three subdomains Ω_i for $i = 1,2,3$ to represent the artery. Let R, Θ and Z be the radius, polar angle and axial distance of a point in the reference domain in cylindrical coordinates and r,θ and z be the corresponding quantities in the deformed domain. We consider (R,Θ,Z) as a generic point in the reference domain and (r,θ,z) as the one in the deformed domain. Suppose $\mathbf{u}$ is the displacement field that maps the reference domain into the deformed domain. The deformation gradient $\mathbf{F}$ is related to $\mathbf{u}$ via

$$\mathbf{F} = \mathbf{I} + \nabla \mathbf{u} \tag{2.24}$$

Then the deformation gradient (2.24) in cylindrical coordinates will be given by

$$\mathbf{F} = \begin{bmatrix} \frac{\partial r}{\partial R} & \frac{1}{R}\frac{\partial r}{\partial \Theta} & \frac{\partial r}{\partial Z} \\ r\frac{\partial \theta}{\partial R} & \frac{r}{R}\frac{\partial \theta}{\partial \Theta} & r\frac{\partial \theta}{\partial Z} \\ \frac{\partial z}{\partial R} & \frac{\partial z}{\partial \Theta} & \frac{\partial z}{\partial Z} \end{bmatrix} \tag{2.25}$$

However, in the axisymmetric case r and z are independent of Θ and θ is independent of R and Z, which simplifies the deformation gradient into

$$\mathbf{F} = \begin{bmatrix} \frac{\partial r}{\partial R} & 0 & \frac{\partial r}{\partial Z} \\ 0 & \frac{r}{R} & 0 \\ \frac{\partial z}{\partial R} & 0 & \frac{\partial z}{\partial Z} \end{bmatrix} \tag{2.26}$$

hence

$$J = \det(\mathbf{F}) = \frac{r}{R}\left(\frac{\partial r}{\partial R}\frac{\partial z}{\partial Z} - \frac{\partial r}{\partial Z}\frac{\partial z}{\partial R}\right) \tag{2.27}$$

The fiber direction vectors in each undeformed layer take the form

$$\mathbf{b}_i(R,Z) = \cos(\varphi_i)\hat{\mathbf{e}}_\Theta + \sin(\varphi_i)\hat{\mathbf{e}}_Z \tag{2.28}$$

where $i = 1,2,3$ corresponds to intima, media and adventitia and φ_i is the angle from Figure 2(c) for each layer. Also $\hat{\mathbf{e}}_\Theta$ and $\hat{\mathbf{e}}_Z$ are the circumferential and axial basis vectors in the reference configuration.

Furthermore, $\mathbf{T}_i = J_{g_i}\frac{\partial W_i}{\partial \mathbf{F}_{e_i}}\mathbf{G}_i^{-T}$ for $i = 1,2,3$. Using (2.5)-(2.8) and (2.27)-(2.28) we have:

$$\begin{aligned} \frac{\partial W_i}{\partial \mathbf{F}_{e_i}} &= \mu_i \mathbf{F}_{e_i} + \frac{2\mu_i \nu (J_{e_i}-1)J_{e_i}}{1-2\nu}\mathbf{F}_{e_i}^{-T} - \mu_i \mathbf{F}_{e_i}^{-T} \\ &+ 4\eta_i \left\{\rho_i \mathbf{F}_{e_i}\mathbf{b}_i\mathbf{b}_i^T (I_4-1)_+ + (1-\rho_i)\mathbf{F}_{e_i}(I_1-3)\right\} e^{\beta_i\left[\rho_i (I_4-1)_+^2 + (1-\rho_i)(I_1-3)^2\right]} \end{aligned} \tag{2.29}$$

As mentioned before the biology of our problem suggests that the growth occurs only inside the intima. Therefore, $\mathbf{G}_i = \mathbf{I}$ and $J_{g_i} = 1$ when $i = 2,3$. On the other hand we consider $\mathbf{G}_1 = \mathrm{diag}(g_\alpha(t,Z), g_\beta(t,Z), g_\gamma(t,Z))$ with

$$g_\alpha(t,Z) = 1 + \alpha t \exp(-aZ^2) \tag{2.30}$$

$$g_\beta(t,Z) = 1 + \beta t \exp(-aZ^2) \tag{2.31}$$

$$g_\gamma(t,Z) = 1 + \gamma t \exp(-aZ^2) \tag{2.32}$$

corresponding to radial, circumferential and axial growth respectively. The variable t is time which is in years throughout this paper. We include the exponential functions in Z to model the effect of local growth in the axial direction. Furthermore, we want growth to increase linearly in time but at different rates and this is the reason for including α,β and γ. In other words, these parameters α,β and γ allow us to explore the effect of anisotropic growth on Glagov remodeling and in the case of isotropic growth we will have $\alpha=\beta=\gamma$. The parameter a determines the locality of growth. We denote the radii of the boundaries between the lumen, intima, media, adventitia and the external tissue in the reference domain by A_1,A_2,A_3 and A_4 respectively. Also the value L specifies the half-length of the artery cross section such that $-L<Z<L$. See Table 1.

We are now ready to propose a weak form for (2.16)-(2.22).

THEOREM 2.1 Suppose a constant pressure load p is applied to the inner boundary $\partial\Omega_1^{(1)}$ of a three layered arterial domain $\Omega=\bigcup_{i=1}^{3}\Omega_i$ with piecewise smooth boundaries. For simplicity we denote the outward unit normal vectors $\mathbf{N}|_{\partial\Omega_i^{(k)}}$, $\mathbf{N}|_{\partial\Omega_L}$ and $\mathbf{N}|_{\partial\Omega_R}$ by $\mathbf{N}_i^{(k)}$, $\mathbf{N}_L$ and $\mathbf{N}_R$ for $i=1,2,3$ and $k=1,2$, respectively. Assume that the domain has a finite length $2L$ and is traction free at both ends and $\mathbf{f}\in L^2(\Omega)$ and $\mathbf{G}_i$ for $i=1,2,3$ are growth tensors defined on the intima, media and adventitia respectively. Then defining $J_{g_i}=\det(\mathbf{G}_i)$ the displacement field $\mathbf{u}\in C^2(\Omega)$ that solves (2.16)-(2.22) also satisfies

$$2\pi\sum_{i=1}^{3}\int_{-L}^{L}\int_{A_i}^{A_{i+1}}\left[\left(J_{g_i}\frac{\partial W_i}{\partial\mathbf{F}_{e_i}}\mathbf{G}_i^{-T}:\nabla\mathbf{v}\right)-\mathbf{f}\cdot\mathbf{v}\right]R\,dR\,dZ$$
$$+2\pi pA_1\left(\int_{-L}^{L}J\mathbf{F}^{-T}\mathbf{N}_1^{(1)}\cdot\mathbf{v}\,dZ\right)=0 \tag{2.33}$$

for every $\mathbf{v}\in C^2(\Omega)$, where $\frac{\partial W_i}{\partial\mathbf{F}_{e_i}}$ is defined in (2.29), J is defined in (2.27) and $\mathbf{F}$ is defined by (2.24) and (2.26).

Proof.

Let $\mathbf{v}\in C^2(\Omega)$. By multiplying both sides of (2.16)-(2.22) by $\mathbf{v}$ and integrating over their respective domains we get

$$\int_{\Omega}(\nabla\cdot\mathbf{T})\cdot\mathbf{v}\mathbf{dx}=-\int_{\Omega}\mathbf{f}\cdot\mathbf{v}\mathbf{dx}, \tag{I}$$
$$\int_{\partial\Omega_1^{(1)}}\mathbf{T}\mathbf{N}_1^{(1)}\cdot\mathbf{v}ds=-\int_{\partial\Omega_1^{(1)}}pJ\mathbf{F}^{-T}\mathbf{N}_1^{(1)}\cdot\mathbf{v}ds, \tag{II}$$
$$\int_{\partial\Omega_3^{(2)}}\mathbf{T}\mathbf{N}_3^{(2)}\cdot\mathbf{v}ds=0, \tag{III}$$
$$\int_{\partial\Omega_1^{(2)}}\mathbf{T}\mathbf{N}_1^{(2)}\cdot\mathbf{v}ds+\int_{\partial\Omega_2^{(1)}}\mathbf{T}\mathbf{N}_2^{(1)}\cdot\mathbf{v}ds=0, \tag{IV}$$
$$\int_{\partial\Omega_2^{(2)}}\mathbf{T}\mathbf{N}_2^{(2)}\cdot\mathbf{v}ds+\int_{\partial\Omega_3^{(1)}}\mathbf{T}\mathbf{N}_3^{(1)}\cdot\mathbf{v}ds=0, \tag{V}$$
$$\int_{\partial\Omega_L}\mathbf{T}\mathbf{N}_L\cdot\mathbf{v}ds=0, \tag{VI}$$
$$\int_{\partial\Omega_R}\mathbf{T}\mathbf{N}_R\cdot\mathbf{v}ds=0. \tag{VII}$$

Adding equations (I)-(VII) and using $\Omega = \bigcup_{i=1}^{3} \Omega_i$ gives us

$$
\begin{aligned}
&-\sum_{i=1}^{3}\left[\int_{\Omega_i}(\nabla\cdot\mathbf{T}_i)\cdot\mathbf{v}\mathbf{dx}\right]-\int_{\Omega}\mathbf{f}\cdot\mathbf{v}\mathbf{dx}+\int_{\partial\Omega_1^{(1)}}pJ\mathbf{F}^{-T}\mathbf{N}_1^{(1)}\cdot\mathbf{v}\mathbf{dx}+\int_{\partial\Omega_1^{(1)}}\mathbf{T}\mathbf{N}_1^{(1)}\cdot\mathbf{v}ds\\
&+\int_{\partial\Omega_2^{(1)}}\mathbf{T}\mathbf{N}_2^{(1)}\cdot\mathbf{v}ds+\int_{\partial\Omega_3^{(1)}}\mathbf{T}\mathbf{N}_3^{(1)}\cdot\mathbf{v}ds+\int_{\partial\Omega_1^{(2)}}\mathbf{T}\mathbf{N}_1^{(2)}\cdot\mathbf{v}ds+\int_{\partial\Omega_2^{(2)}}\mathbf{T}\mathbf{N}_2^{(2)}\cdot\mathbf{v}ds\\
&+\int_{\partial\Omega_3^{(2)}}\mathbf{T}\mathbf{N}_3^{(2)}\cdot\mathbf{v}ds+\int_{\partial\Omega_L}\mathbf{T}\mathbf{N}_L\cdot\mathbf{v}ds+\int_{\partial\Omega_R}\mathbf{T}\mathbf{N}_R\cdot\mathbf{v}ds=0
\end{aligned}
\tag{2.34}
$$

Now using the divergence theorem on the sum results in

$$
\begin{aligned}
-\sum_{i=1}^{3}\left[\int_{\Omega_i}(\nabla\cdot\mathbf{T}_i)\cdot\mathbf{v}\mathbf{dx}\right]=\sum_{i=1}^{3}\left[\int_{\Omega_i}(\mathbf{T}_i:\nabla\mathbf{v})\mathbf{dx}\right]&-\int_{\partial\Omega_1^{(1)}}\mathbf{T}\mathbf{N}_1^{(1)}\cdot\mathbf{v}ds-\int_{\partial\Omega_2^{(1)}}\mathbf{T}\mathbf{N}_2^{(1)}\cdot\mathbf{v}ds\\
&-\int_{\partial\Omega_3^{(1)}}\mathbf{T}\mathbf{N}_3^{(1)}\cdot\mathbf{v}ds-\int_{\partial\Omega_1^{(2)}}\mathbf{T}\mathbf{N}_1^{(2)}\cdot\mathbf{v}ds-\int_{\partial\Omega_2^{(2)}}\mathbf{T}\mathbf{N}_2^{(2)}\cdot\mathbf{v}ds\\
&-\int_{\partial\Omega_3^{(2)}}\mathbf{T}\mathbf{N}_3^{(2)}\cdot\mathbf{v}ds-\int_{\partial\Omega_L}\mathbf{T}\mathbf{N}_L\cdot\mathbf{v}ds-\int_{\partial\Omega_R}\mathbf{T}\mathbf{N}_R\cdot\mathbf{v}ds
\end{aligned}
\tag{2.35}
$$

By replacing (2.35) in (2.34) we get

$$
\sum_{i=1}^{3}\left[\int_{\Omega_i}(\mathbf{T}_i:\nabla\mathbf{v})\mathbf{dx}\right]-\int_{\Omega}\mathbf{f}\cdot\mathbf{v}\mathbf{dx}+\int_{\partial\Omega_1^{(1)}}pJ\mathbf{F}^{-T}\mathbf{N}\cdot\mathbf{v}ds=0 \tag{2.36}
$$

Switching to cylindrical coordinates we get

$$
2\pi\sum_{i=1}^{3}\left[\int_{-L}^{L}\int_{A_i}^{A_{i+1}}\left[(\mathbf{T}_i:\nabla\mathbf{v})-\mathbf{f}\cdot\mathbf{v}\right]\,R\,dR\,dZ\right]+2\pi\left(\int_{-L}^{L}pJ\mathbf{F}^{-T}\mathbf{N}\cdot\mathbf{v}\,R\,dZ\right)\Big|_{R=A_1}=0
$$

Notice that since there is no dependence on Θ due to axisymmetry we have integrated with respect to Θ producing the 2π coefficients. Using the definition $\mathbf{T}_i = J_{g_i}\frac{\partial W_i}{\partial \mathbf{F}_{e_i}}\mathbf{G}_i^{-T}$ we get (2.33) for every $\mathbf{v}\in C^2(\Omega)$. □

Note: In this paper we assume that the body forces are negligible. Therefore, (2.33) turns into

$$
2\pi\sum_{i=1}^{3}\int_{-L}^{L}\int_{A_i}^{A_{i+1}}\left(J_{g_i}\frac{\partial W_i}{\partial\mathbf{F}_{e_i}}\mathbf{G}_i^{-T}:\nabla\mathbf{v}\right)\,R\,dR\,dZ+2\pi\left(p\int_{-L}^{L}J\mathbf{F}^{-T}\mathbf{N}\cdot\mathbf{v}\,R\,dZ\right)\Big|_{R=A_1}=0 \tag{2.37}
$$

for every $\mathbf{v}\in C^{\infty}(\Omega)$. We use the following table for parameter values.

Symbol	Units	Value
μ_1	kPa	27.9
μ_2	kPa	1.27
μ_3	kPa	7.56
ν	Dimensionless	0.49
η_1	kPa	263.66
η_2	kPa	21.60
η_3	kPa	38.57
β_1	Dimensionless	170.88
β_2	Dimensionless	8.21
β_3	Dimensionless	85.03
ρ_1	Dimensionless	0.51
ρ_2	Dimensionless	0.25
ρ_3	Dimensionless	0.55
φ_1	Degrees	60.3
φ_2	Degrees	20.61
φ_3	Degrees	67
A_1	mm	1.26
A_2	mm	1.47
A_3	mm	1.89
A_4	mm	2.31
L	cm	3.36

Table 1: List of parameter values used in this paper. All the values are proposed by Holzapfel et al. (2005) as a result of experimenting on 13 hearts from 3 women and 10 men post mortem.

Ultimately, we need to find a displacement field $\mathbf{u}$ that gives us a deformation gradient $\mathbf{F}$ in (2.24) and (2.26) which gives us the elastic tensors $\mathbf{F}_{e_i} = \mathbf{F}\mathbf{G}^{-1}$ for each layer by (2.1) which leads to the first Piola-Kirchoff stress tensors $\mathbf{T}_i$ for each layer that satisfies (2.37) for sufficiently smooth $\mathbf{v}$.

We use FEniCS as our computing platform for solving this problem numerically. FEniCS is a powerful open source package that can be utilized by languages such as C++ and Python (Langtangen et al. (2016)). For this problem we use a 2D mesh in (R,Z) with about 11000 triangles, see Fig 3. To avoid shear locking we use second order elements. This way we approximate the displacement field by second order Lagrangian elements which leads to a linear approximation for the strain. Also increasing the number of elements along the thickness of the domain is another common remedy for shear locking (Zienkiewicz & Taylor (2005)). Although the problem is computationally intensive, the University of Delaware's Caviness cluster was able to find solutions in about 12 hours. Thanks to access to a high performance computing resource we were able to simulate growth for values of t as large as 3 decades in (2.30)-(2.32).

3. Results and Discussion

For the rest of this paper we consider the blood pressure to be the static average value between systolic and diastolic blood pressure with $p = 16$ kPa $= 120$mmHg and we assume that the artery is in the pressurized state at $t = 0$, see Figure 3. To focus on the effect of growth on the arterial remodeling and Glagov phenomenon, we neglect the dynamic changes in the blood pressure. The blood pressure causes

the radii A_1, A_2, A_3 and A_4 to increase and as a result the length of the artery decreases to conserve the volume. In the special case where $\eta = 0$ in (2.6) for each layer, validation was done by comparing the results of our Fenics code with a 1D solution (solved using Matlab), see the appendix in Fok & Gou (2020). Signs of coronary artery disease rarely occur in young adults (age < 40) (Tsai et al. (2017)) and stenosis larger than 50% is often observed in adults older than 60 (Giannoglou et al. (2006))). Therefore, we assume in our model atherosclerosis starts around age 35 and continues until 65, and we run our simulations from $t = 0$ to $t = 30$ years accordingly.

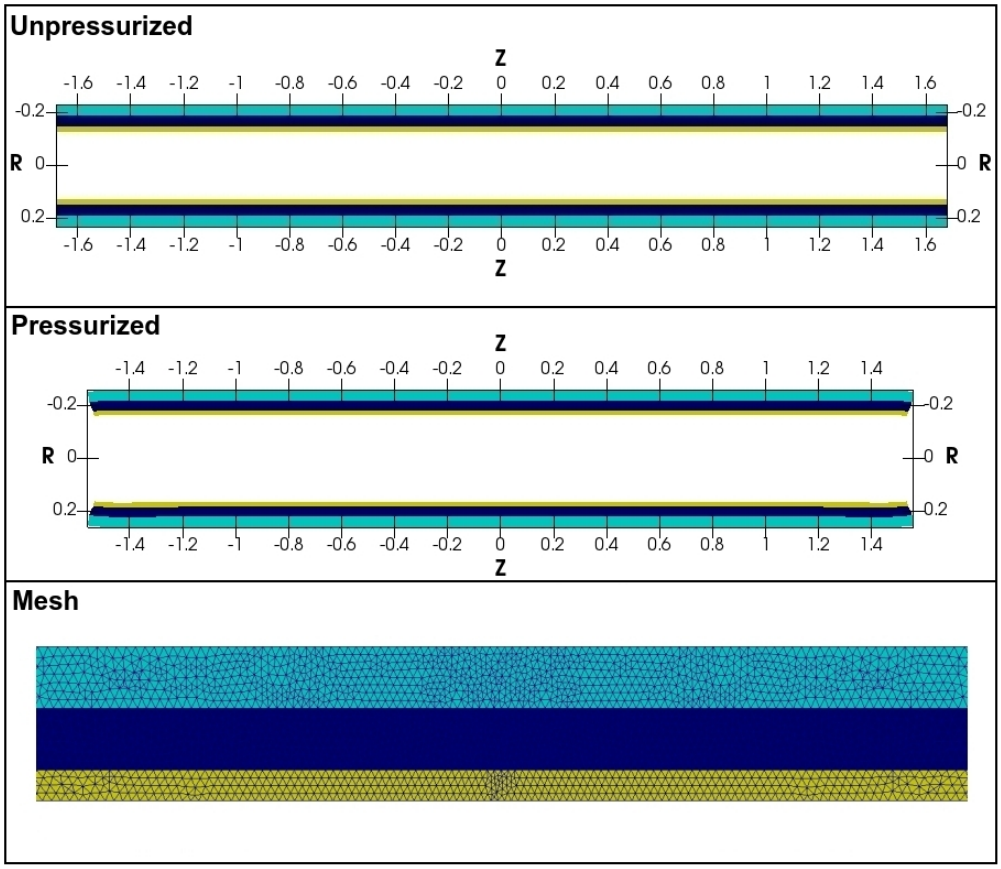

FIG. 3: *Top*: The unpressurized reference domain. *Middle*: The reference domain after applying the blood pressure of 16 kPa. *Bottom*: Mesh sample for $-0.58 \leqslant Z \leqslant 0.58$. Mesh is denser where growth is larger.

3.1 *The effect of pure growth in each direction*

First we start with investigating the effect of pure growth in the radial, circumferential and axial directions. We can roughly see in Figure 4 the effect of such growth. We believe that their different behaviors will give insight on how each component of the growth tensor contributes to the overall process of remodeling. We provide graphs such as lumen area as a function of stenosis and lumen area as a function

of time given the definition

$$\text{Stenosis}(Z) = \frac{\text{Intima Area}(Z)}{\text{Intima Area}(Z) + \text{Lumen Area}(Z)} \tag{3.1}$$

where Stenosis(Z), Intima Area(Z) and Lumen Area(Z) correspond to the stenosis, intima area and lumen area at axial position Z respectively. In addition, we explore changes in the fiber angles and total energy.

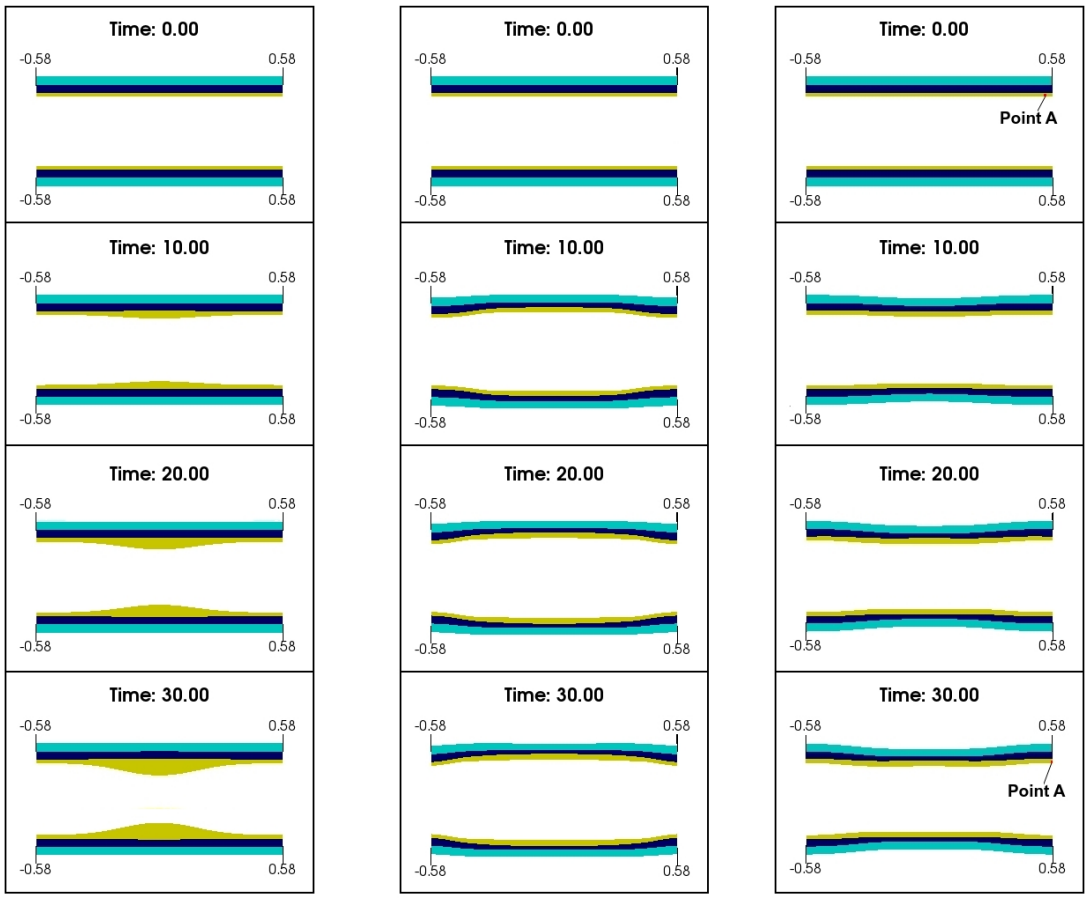

FIG. 4: Evolution of the domain for $-0.58 \leqslant Z \leqslant 0.58$ subject to (a) pure radial growth with $(\alpha,\beta,\gamma) = (1,0,0)$, (b) pure circumferential growth with $(\alpha,\beta,\gamma) = (0,1,0)$ and (c) pure axial growth with $(\alpha,\beta,\gamma) = (0,0,1)$. The material point at A moves to the right under the effect of axial growth. Parameter a in (2.30)-(2.32) is taken to be 14.29.

3.1.1 *Pure Radial Growth,* Let us assume that the intima grows according to the growth tensor $\mathbf{G}_\alpha = \text{diag}(g_\alpha(t,Z),1,1)$. This means that the intima grows radially by $g_\alpha(t,Z)$ from (2.30) and there is no growth in the circumferential and radial direction.

According to Figure 4(a) the radial growth almost exclusively contributes to inward thickening of the intima. As expected the inward remodeling is greater when closer to the center of growth $Z = 0$ and consequently the artery undergoes more stenosis there, see Figure 5. We refrained from including more cross sections since far away from $Z = 0$ the growth function has little to no effect and therefore the lumen area stays the same. We will also see that pure radial growth does not greatly affect the total energy, see section 3.2.

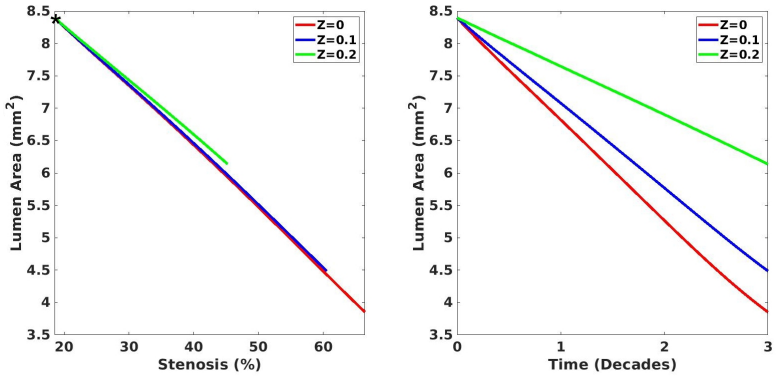

FIG. 5: *Left*: Lumen area against stenosis. Star denotes the time $t = 0$. *Right*: Lumen area in time. With pure radial growth close to the center of growth $Z = 0$ the remodeling is strictly inward.

3.1.2 *Pure Circumferential Growth,* Now we assume that growth is purely in the circumferential direction. Therefore the growth tensor takes the form $\mathbf{G}_\beta = \mathrm{diag}(1, g_\beta(t,Z), 1)$.

According to Figure 4(b), pure circumferential growth mostly contributes to the outward remodeling of the vessel. There is a slight intimal thickening and increase in stenosis but compared to the radial growth it is negligible, see Figure 6. Also one can see that the lumen area plateaus in Figure 6 for large t which might be due to the effect of stiffening collagen fibers.

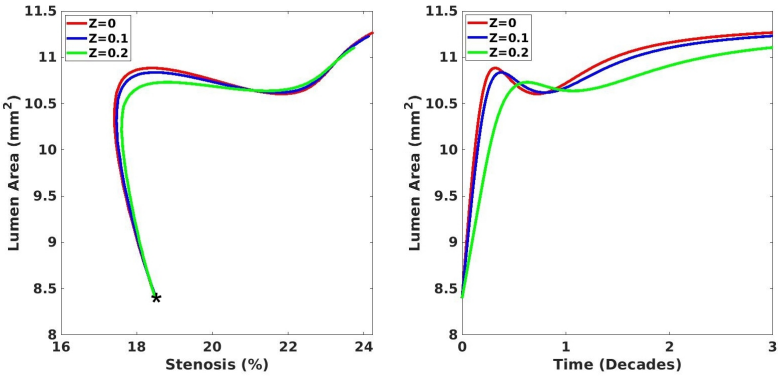

FIG. 6: *Left*: Lumen area against stenosis. Star denotes the time $t = 0$. *Right*: Lumen area in time. With pure circumferential growth close to the center of growth $Z = 0$ the remodeling is mostly outward.

3.1.3 *Pure Axial Growth,* Finally we do the same investigation when growth is purely in the axial direction. Therefore we take the growth tensor to be $\mathbf{G}_\gamma = \text{diag}(1,1,g_\gamma(t,Z))$.

Pure axial growth mainly contributes to axial elongation, see Figure 4(c). We see a short outward remodeling followed by a significant inward remodeling for this type of growth, see Figure 7. However, unlike the pure radial growth remodeling is not exclusively a result of intimal thickening. As one can see in Figure 4(c), the intima thickness is not significant but we can see a mild inward buckling of the arterial wall which reduces the lumen area. We have seen the effects of growth in the radial, circumferential and axial directions. Now we explore the energy change associated with each of these growth modes.

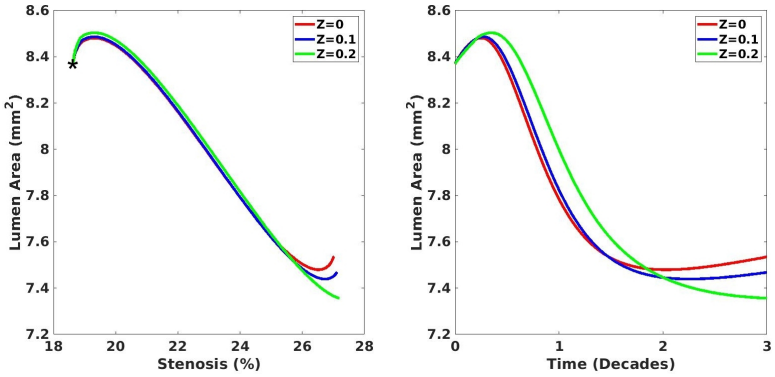

FIG. 7: *Left*: Lumen area against stenosis. Star denotes the time $t = 0$. *Right*: Lumen area in time. With pure axial growth close to the center of growth $Z = 0$ the remodeling is mostly outward with no significant increase in stenosis.

3.2 *Growth and Energy Change*

In this section we are interested in calculating the energy change in the artery due to each growth direction. We want to see which growth direction is more energetically favorable. The total energy consists of the bulk energy and the energy produced by the external forces such as the blood pressure.

$$E = \underbrace{2\pi \sum_{i=1}^{3} \int_{-L}^{L} \int_{A_i}^{A_{i+1}} J_{g_i} W_i \, R \, dR \, dZ}_{\text{Energy due to volumetric strain caused by growth}} \underbrace{+ 2\pi A_1 \frac{p}{3} \int_{-L}^{L} J\mathbf{F}^{-\mathbf{T}} \mathbf{N}_\mathbf{1}^{(\mathbf{1})} \cdot \mathbf{u} \, dZ}_{\text{Energy due to blood pressure}}, \tag{3.2}$$

where W_i is defined as $\Psi^i_{\text{iso}} + \Psi^i_{\text{aniso}}$ from (2.5) and (2.6).

THEOREM 3.1 The displacement field $\mathbf{u} \in C^2(\Omega)$ that satisfies the weak equation

$$2\pi \sum_{i=1}^{3} \int_{-L}^{L} \int_{A_i}^{A_{i+1}} \left(J_{g_i} \frac{\partial W_i}{\partial \mathbf{F}_{e_i}} \mathbf{G}_i^{-T} : \nabla \mathbf{v} \right) R \, dR \, dZ + 2\pi p A_1 \left(\int_{-L}^{L} J\mathbf{F}^{-T} \mathbf{N}_1^{(1)} \cdot \mathbf{v} \, dZ \right) = 0 \tag{3.3}$$

for every $\mathbf{v} \in C^2(\Omega)$ also makes (3.2) stationary. Note that equation (3.3) is just equation (2.33) in the special case when $\mathbf{f} = 0$.

Proof. For a proof refer to Fok & Gou (2020). □

Now to observe the change in energy purely imposed by growth in each direction we compute the

total energy (3.2) for the three cases in sections 3.1.1, 3.1.2 and 3.1.3. The result is shown in Figure 8. We extract the energies induced by each growth direction at times $t = 5, 10, 15, 20, 25, 30$ from Figure 8, and show them in Table 2. Assuming that intima growth stems from cell division, the amount of energy needed for the cells to divide in the radial direction is much less than the energy in the circumferential and axial directions. In other words, it takes about 3 years for the axial growth to produce the same energy as the radial growth does in 30 years. For circumferential growth, it is 5 years. Therefore, growing in the axial direction is energetically the least favorable while growing in the radial direction is energetically the most favorable. This observation motivates the need for an anisotropic treatment of the growth process.

Direction \ Time	t=5	t=10	t=15	t=20	t=25	t=30	Average
Radial	0.3669	0.3670	0.3670	0.3671	0.3671	0.3672	0.3670
Circumferential	0.3671	0.4648	0.7930	1.452	2.435	3.701	1.5355
Axial	0.4075	0.6262	1.1760	2.1140	3.3940	4.9520	2.1116

Table 2: Energy in μJ for 6 time values.

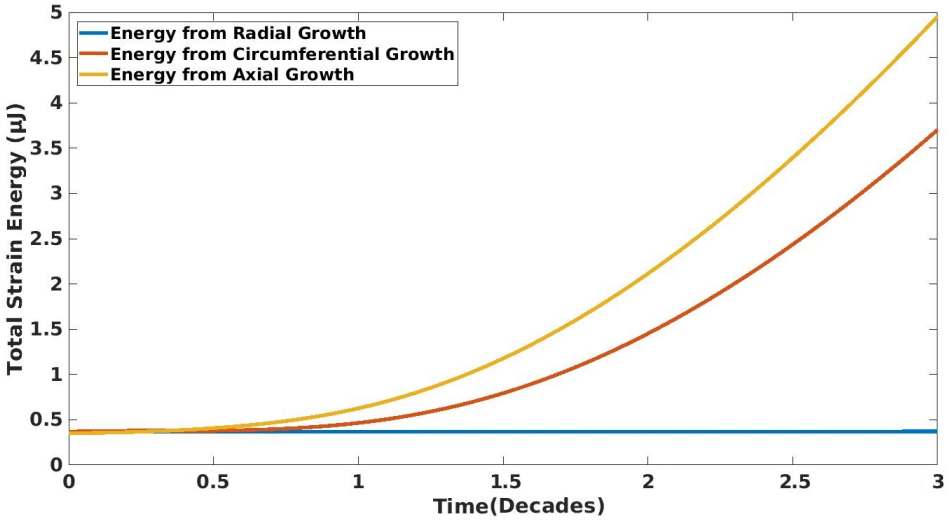

FIG. 8: Components of the growth tensor $\mathbf{G}$ at $Z = 0$ in the anisotropic and isotropic cases. For the anisotropic case at $Z = 0$, $\mathbf{G} = \text{diag}(1+\alpha_t t, 1+\beta_t t, 1+\gamma_t t)$. For the isotropic case at $Z = 0$, $\mathbf{G} = \text{diag}(1+\xi_t t, 1+\xi_t t, 1+\xi_t t)$. The growth parameters $\alpha_t, \beta_t, \gamma_t$ were found by minimizing the total energy and xi_t was found by ensuring $\det(\mathbf{G})$ was equal at $Z = 0$ in both cases.

3.3 *Isotropic Growth vs General Anisotropic Growth*

Motivated by the previous section, here we discuss a method to choose an anisotropic growth that is energetically most favorable. We hypothesize that such method will give a growth tensor that has a large weight in the radial component. Our method is inspired by the common two field minimization for incompressible materials. However, instead of minimizing for a displacement and pressure field we

minimize with respect to displacement and growth. Mathematically, we want to find $\mathbf{u}$ and $(\alpha_t, \beta_t, \gamma_t)$ that minimizes (3.2) subject to

$$J_{g_1} = f(t), \qquad \text{at} \quad Z = 0 \tag{3.4}$$

where $\alpha_t, \beta_t, \gamma_t$ are the parameters in (2.30), (2.31), (2.32). The subscript t is to emphasize that the minimization happens at each time-step to produce a displacement vector field and three growth parameters. The constraint (3.4) can be imposed by letting γ_t be a function of α_t and β_t as follows

$$\gamma_t = \frac{\frac{f(t)}{(1+\alpha_t t)(1+\beta_t t)} - 1}{t}, \tag{3.5}$$

This ensures that (3.4) will hold. The function $f(t)$ is set by the user in this scheme to determine the desired volumetric growth at each step (in our simulations we use $f(t) = 1 + 2.7t$). After this, to show the importance of using an anisotropic growth scheme as opposed to an isotropic scheme we compare the two cases. For the isotropic growth tensor $\text{diag}(1 + \xi_t t \exp(-aZ^2), 1 + \xi_t t \exp(-aZ^2), 1 + \xi_t t \exp(-aZ^2))$ we choose ξ_t such that

$$\xi_t = \frac{\sqrt[3]{f(t)} - 1}{t} \tag{3.6}$$

This choice of ξ_t will ensure that the Jacobian of the growth tensor for both cases are equal at $Z = 0$ at each time t. Figure 9 shows $1 + \xi_t t$ as well as $1 + \alpha_t t$, $1 + \beta_t t$ and $1 + \gamma_t t$ acquired form the two field minimization problem conditional on (3.4).

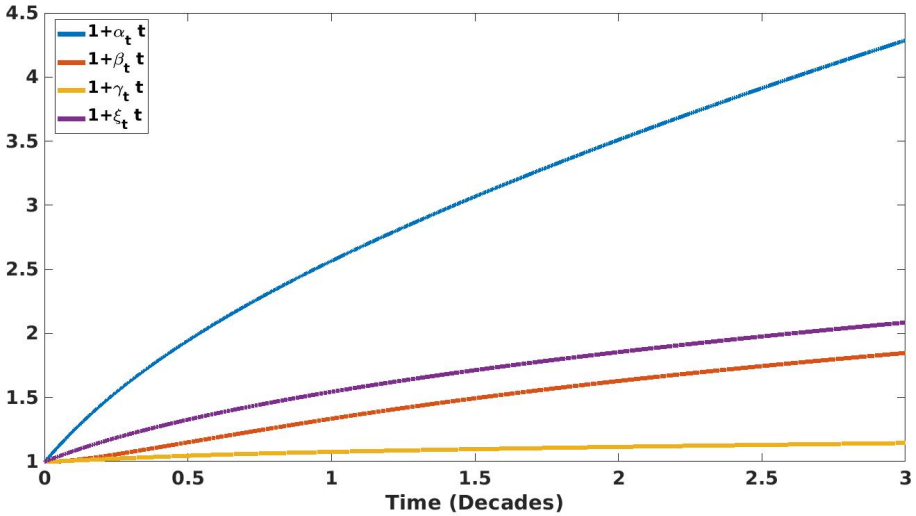

FIG. 9: Changes in anisotopic growth parameters $\alpha_t, \beta_t, \gamma_t$ and isotropic growth parameter ξ_t.

From Figure 9, one can see that this minimization produces a growth regime in which the radial component is dominant. This is not surprising since the energy is very insensitive to radial growth, see Figure 8. The axial direction as expected from Figure 8 is the most strictly controlled growth direction.

Now using the growth parameters from Figure 9 at each time step, we acquire the evolution of the domain in time, Figure 10. We observe a mild buckling effect in the isotropic case which can be due to the axial stress in each layer. In addition, the intima is thickened but the narrowing of the lumen is not completely a result of intimal thickening in this case. It is clear that buckling contributes to the narrowing process. On the other hand, for anisotropic growth with approximately the same J_g we can clearly observe an intimal thickening close to the center of growth as the main contributor to the encroachment. Figure 11 shows that the isotropic growth induces much less stenosis compared to the anisotropic growth. On the other hand, the behavior of the lumen area vs stenosis curves in the anisotropic case (specifically at $Z = 0$) look very similar to Glagov's original data (Glagov et al. (1987)). Finally a comparison between the energies from the isotropic and anisotropic growth shows that the latter is much more energetically favorable, see Figure 12.

In addition, we investigate the changes in the fiber angles and values of I_4 in (2.8). The latter can be thought as a measurement of stiffness for each layer. In both isotropic and anisotropic cases, the fiber angle in the intima increases the most, see Figure 13(a) and (c). However, Figures 13 (b) and (d) show that I_4 does not change significantly in the intima in both cases. Physically this means the fibers do not change their length in the intima, only their orientation. In addition, Figures 13 (b) and (d) show that the isotropic case eventually a stiffer adventitia but a more compliant media than the anisotropic case. Therefore, the intima in the anisotropic case finds it easier growing inward than pushing against a stiffer media to grow outward. This is supported by the difference in the sizes of the inward bulges in the two cases in Figure 11.

Finally, we impose our energetically favorable anisotropic growth scheme on arteries with different initial lumen areas. Figure 14 shows the lumen area-stenosis curves for six arteries at $Z = 0$ along with Glagov's original data. This further confirms that our energetically favorable anisotropic growth model is a better fit for real data than the isotropic case.

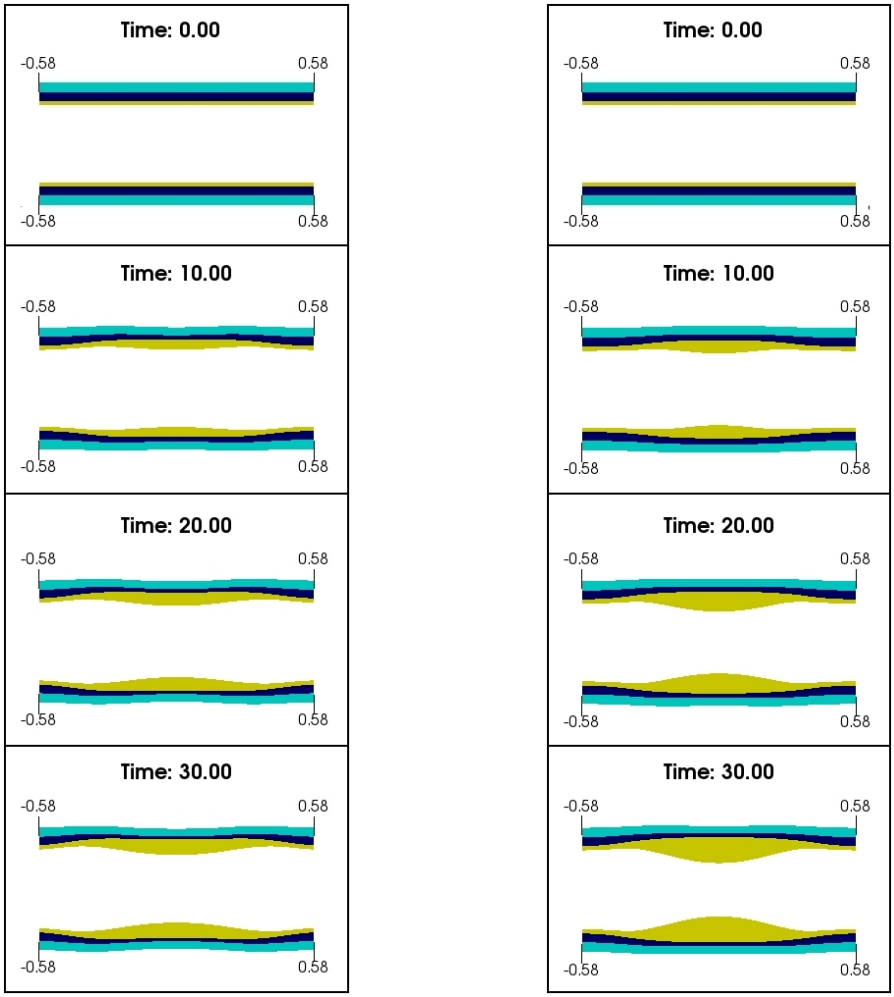

(a) (b)

FIG. 10: Evolution of the domain for $-0.58 \leqslant Z \leqslant 0.58$ subject to (a) isotropic growth with ξ_t from Fig. 9, (b) general anisotropic growth with $(\alpha_t, \beta_t, \gamma_t)$ from Fig. 9. Parameter a in (2.30)-(2.32) is taken to be 14.29.

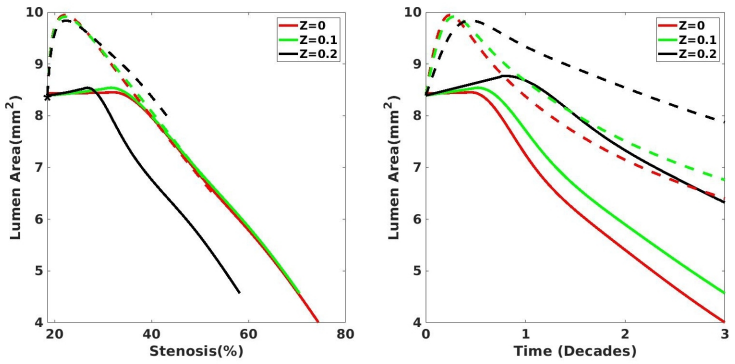

FIG. 11: *Left*: Comparison between the lumen area against stenosis for both isotropic and anisotropic growth. Star denotes the time $t = 0$. *Right*: Comparison between the lumen area in time for both isotropic and anisotropic growth. *Dashed* lines correspond to isotropic and *solid* lines correspond to anisotropic growth.

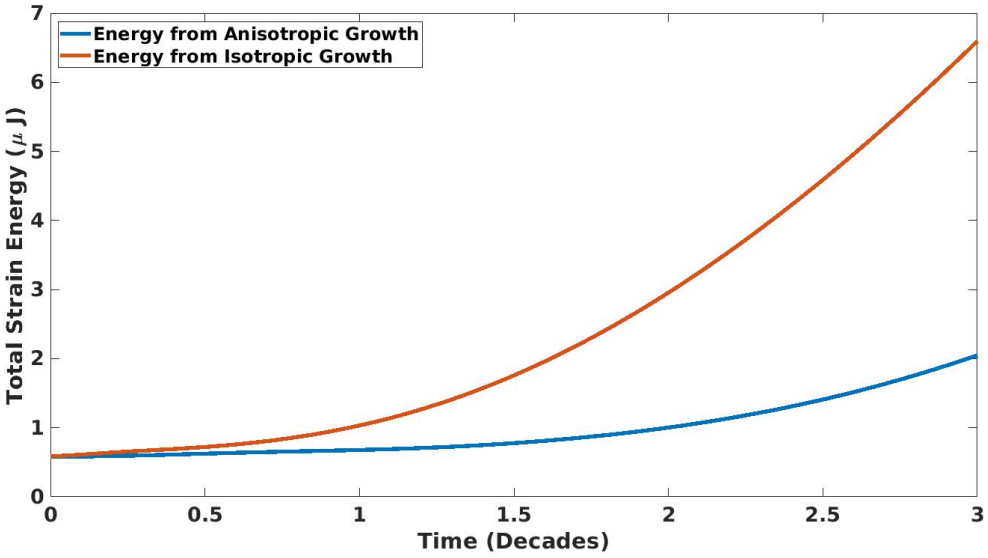

FIG. 12: Changes in the strain energy produced by isotropic and anisotropic growth in time.

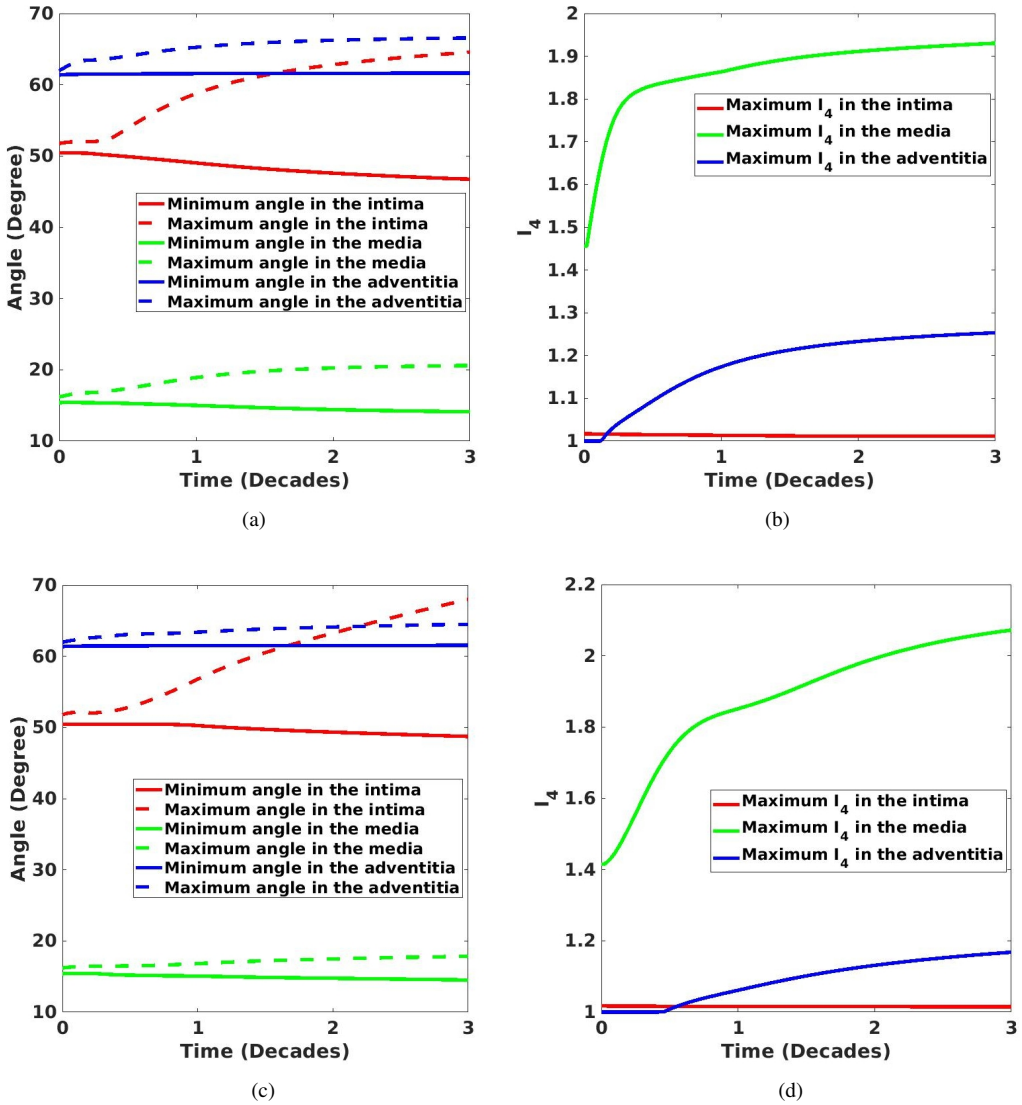

FIG. 13: *Top:* Isotropic growth with ξ_t from Fig. 9. (a) Changes in the minimum and maximum fiber angles. (b) Changes in the maximum of I_4 in each layer.
Bottom: Anisotropic growth with $(\alpha_t, \beta_t, \gamma_t)$ from Fig. 9. (c) Changes in the minimum and maximum fiber angles. (d) Changes in the maximum of I_4 in each layer.

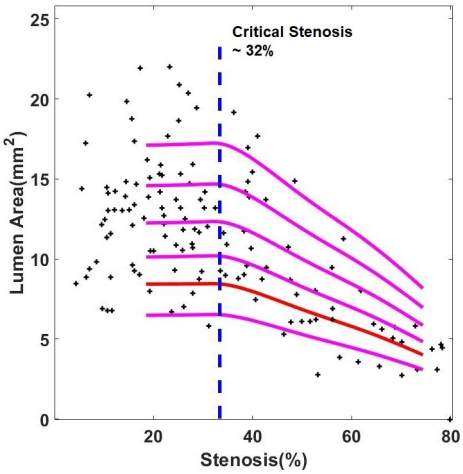

FIG. 14: Glagov curves at $Z = 0$ for six arteries under anisotropic growth. For each case, all linear dimensions for the artery were scaled by a factor ζ. Each curve corresponds to a 10% increase in arterial dimensions, that is, $\zeta = 0.9, 1.0, 1.1, 1.2, 1.3, 1.4$ respectively. Stenosis is unchanged by the scaling while lumen area increases by ζ^2. The red curve corresponds to the one in Figure 11. The data points are Glagov's original data and the dashed blue line marks the begining of inward remodeling.

4. Conclusion

In this paper we investigated an axisymmetric growing artery using morphoelasticity. First we were curious to see the effect of growth in each direction separately. This allowed us to associate each aspect of the Glagov remodeling phenomenon with growth in a certain direction. We observed that the radial growth is the main culprit in encroachment of the vessel while circumferential growth is responsible for the outward remodeling. In the case of axial growth, we saw both types of remodeling. However, the inward remodeling was partly a result of arterial wall buckling. We also saw that radial growth thickens the intima without changing the thickness of the other two layers. The circumferential growth thins the media and thickens the intima slightly, and the axial growth slightly thickens the intima and, thins the media and stretches the artery axially.

We hypothesized that if the growth tensor is determined by an energy minimization, radial growth would emerge to become dominant. We suggested a displacement-growth two field minimization framework to test our hypothesis. As we expected due to the large energy produced by axial and circumferential growth this prescription suppresses the effect of these growth directions. In other words, for the growth tensor

$$\mathbf{G} = \mathrm{diag}(1 + \alpha_t t \exp(-aZ^2), 1 + \beta_t t \exp(-aZ^2)), 1 + \gamma_t t \exp(-aZ^2))$$

the parameters α_t, β_t and γ_t follow $\alpha_t > \beta_t > \gamma_t$ for the most part.

To further enforce the need for an anisotropic treatment of our problem we investigated an isotropic growth with the growth tensor

$$\mathbf{G} = \mathrm{diag}(1 + \xi_t t \exp(-aZ^2), 1 + \xi_t t \exp(-aZ^2)), 1 + \xi_t t \exp(-aZ^2))$$

The parameter ξ_t is chosen such that the maximum Jacobian of growth (which happens at $Z = 0$) for both cases is exactly the same for each time step t. Our result is that the anisotopic growth is much

more energetically favorable than the isotropic case for the same amount of volumetric growth. On a plot of lumen area vs stenosis, anisotropic growth produced curves that were closer to Glagov's original data. Furthermore, we saw more stenosis for the more energetically favorable anisotropic growth than isotropic growth. This was expected due to the dominance of growth in the radial direction and the increased effective stiffness of the media layer in the anisotropic case.

Many studies have shown that smooth muscle cell (SMC) proliferation is the reason for intimal thickening (Groves et al. (1995), Sho et al. (2002), Francis et al. (2003) and Nakagawa & Nakashima (2018)). In addition, there are studies that suggest that SMC proliferation is regulated by changes in the circumferential stress in the vessel wall (Wayman et al. (2008)) or changes in wall shear stress induced by blood flow (Ueba et al. (1997) and Haga et al. (2003)). Although it is acknowledged that atherosclerosis proceeds because of growth in the intima, few authors have studied the nature of the anisotropy in the growth tensor when they model this phenomenon. Our approach was to choose an anisotropic growth tensor based on minimizing the total energy. The result was a radially dominant growth, consistent with experiments on radial construction in arterial walls (Greif et al. (2012)). According to Greif et al. (2012), smooth muscle cells (SMCs) have to re-orient themselves to become "bricks" in the vessel wall. Cells in different layers re-orient themselves at different times, so that there is a re-orientation wave that radiates outwards. This radial patterning is probably due to a platelet derived growth factor (PDGF) wave that itself has a strong radial component. In this paper we do not work with PDGF, but it would be interesting to compute the effective growth tensor from Greif et al. (2012) experiments and compare them with our model predictions.

Our model is consistent with durotaxis (migration of cells up the rigidity gradients in the extracellular matrix), in the sense that growth occurs in the intima only, which is the stiffest layer in atherosclerotic arteries (note that $\eta_1 \gg \eta_2$, η_3 and $\beta_1 \gg \beta_2, \beta_3$ in Table 1). In the early stages of atherosclerosis, smooth muscle cells from the media migrate to the intima and then proliferate. Our model lumps both of these processes into a single growth tensor, $\mathbf{G}$.

In this paper, we did not consider long term dynamics of the blood flow. Our model solely focuses on the arterial remodeling caused by growth. However, in reality, the remodeling process can be significantly affected by hemodynamics due to the sensitivity of endothelial cells to shear stress. Altered laminar shear stress from a flow rate can contribute to the remodeling process (Langille (1996)).Furthermore, it has been observed that a chronic reduction in blood flow can lead to a reduction of the arterial diameter (Langille & O'Donnell (1986)). Therefore, a more realistic model requires a more detailed inclusion of the blood flow rather than a static value.

Even though our hypothesis was tested using the mathematical tool of energy minimization, we hope it can motivate a rigorous biological experiment to validate it. With advances in nanospring technology, it may eventually be possible to measure the energy associated with growth in radial, circumferential and axial directions (Iwaki et al. (2016)). We believe that finding a practical way to control or change the dominant anisotropy of growth might be the key to slow down or even reverse inward remodeling which is responsible for affecting local hemodynamics and promoting medical conditions such as angina.

Acknowledgements: NMM was supported by a DE-CTR SHoRe pilot grant NIGMS IDeA U54-GM104941. PWF was supported by a Simons Foundation collaboration grant, award number 282579.

References

Amar, M. B. & Goriely, A. (2005), 'Growth and instability in elastic tissues', *Journal of the Mechanics and Physics of Solids* **53**(10), 2284–2319.

Antman, E. M. (2007), *Cardiovascular therapeutics: a companion to Braunwald's Heart disease*, Elsevier Health Sciences.

Baek, S. & Pence, T. (2011), 'Inhomogeneous deformation of elastomer gels in equilibrium under saturated and unsaturated conditions', *Journal of the Mechanics and Physics of Solids* **59**(3), 561–582.

Benjamin, E. J., Muntner, P. & Bittencourt, M. S. (2019), 'Heart disease and stroke statistics-2019 update: a report from the american heart association', *Circulation* **139**(10), e56–e528.

Chalmers, A. D., Bursill, C. A. & Myerscough, M. R. (2017), 'Nonlinear dynamics of early atherosclerotic plaque formation may determine the efficacy of high density lipoproteins (hdl) in plaque regression', *PloS one* **12**(11), e0187674.

Chalmers, A. D., Cohen, A., Bursill, C. A. & Myerscough, M. R. (2015), 'Bifurcation and dynamics in a mathematical model of early atherosclerosis', *Journal of mathematical biology* **71**(6-7), 1451–1480.

Channon, K. M. (2006), 'The endothelium and the pathogenesis of atherosclerosis', *Medicine* **34**(5), 173–177.

Davies, M. (1992), 'Anatomic features in victims of sudden coronary death. coronary artery pathology.', *Circulation* **85**(1 Suppl), I19–24.

Demiray, H. & Vito, R. P. (1991), 'A layered cylindrical shell model for an aorta', *International Journal of Engineering Science* **29**(1), 47–54.

El Khatib, N., Génieys, S., Kazmierczak, B. & Volpert, V. (2012), 'Reaction–diffusion model of atherosclerosis development', *Journal of mathematical biology* **65**(2), 349–374.

El Khatib, N., Genieys, S. & Volpert, V. (2007), 'Atherosclerosis initiation modeled as an inflammatory process', *Mathematical Modelling of Natural Phenomena* **2**(2), 126–141.

Fok, P.-W. (2016), 'Multi-layer mechanical model of glagov remodeling in coronary arteries: differences between in-vivo and ex-vivo measurements', *PloS one* **11**(7), e0159304.

Fok, P.-W. & Gou, K. (2020), 'Finite element simulation of intimal thickening in 2d multi-layered arterial cross sections by morphoelasticity', *Computer Methods in Applied Mechanics and Engineering* **363**, 112860.

Fok, P.-W. & Sanft, R. (2017), 'A biochemical and mechanical model of injury-induced intimal thickening', *Mathematical medicine and biology: a journal of the IMA* **34**(1), 77–108.

Francis, D. J., Parish, C. R., McGarry, M., Santiago, F. S., Lowe, H. C., Brown, K. J., Bingley, J. A., Hayward, I. P., Cowden, W. B., Campbell, J. H. et al. (2003), 'Blockade of vascular smooth muscle cell proliferation and intimal thickening after balloon injury by the sulfated oligosaccharide pi-88: phosphomannopentaose sulfate directly binds fgf-2, blocks cellular signaling, and inhibits proliferation', *Circulation research* **92**(8), e70–e77.

Gasser, T. C. & Holzapfel, G. A. (2007), 'Modeling plaque fissuring and dissection during balloon angioplasty intervention', *Annals of biomedical engineering* **35**(5), 711–723.

Giannoglou, G. D., Antoniadis, A. P., Chatzizisis, Y. S., Damvopoulou, E., Parcharidis, G. E. & Louridas, G. E. (2006), 'Prevalence of narrowing >= 50% of the left main coronary artery among 17,300 patients having coronary angiography', *The American journal of cardiology* **98**(9), 1202–1205.

Glagov, S., Weisenberg, E., Zarins, C. K., Stankunavicius, R. & Kolettis, G. J. (1987), 'Compensatory enlargement of human atherosclerotic coronary arteries', *New England Journal of Medicine* **316**(22), 1371–1375.

Goriely, A. & Amar, M. B. (2007), 'On the definition and modeling of incremental, cumulative, and continuous growth laws in morphoelasticity', *Biomechanics and Modeling in Mechanobiology* **6**(5), 289–296.

Greif, D. M., Kumar, M., Lighthouse, J. K., Hum, J., An, A., Ding, L., Red-Horse, K., Espinoza, F. H., Olson, L., Offermanns, S. et al. (2012), 'Radial construction of an arterial wall', *Developmental cell* **23**(3), 482–493.

Groves, P. H., Banning, A. P., Penny, W. J., Lewis, M. J., Cheadle, H. A. & Newby, A. C. (1995), 'Kinetics of smooth muscle cell proliferation and intimal thickening in a pig carotid model of balloon injury', *Atherosclerosis* **117**(1), 83–96.

Gurtin, M. E. (1981), *Topics in finite elasticity*, Vol. 35, SIAM.

Haga, M., Yamashita, A., Paszkowiak, J., Sumpio, B. E. & Dardik, A. (2003), 'Oscillatory shear stress increases smooth muscle cell proliferation and akt phosphorylation', *Journal of vascular surgery* **37**(6), 1277–1284.

Hao, W. & Friedman, A. (2014), 'The ldl-hdl profile determines the risk of atherosclerosis: a mathematical model', *PloS one* **9**(3), e90497.

Holzapfel, G. A. (2000), *Nonlinear Solid Mechanics: A Continuum Approach for Engineering*, Wiley.

Holzapfel, G. A., Gasser, T. C. & Ogden, R. W. (2000), 'A new constitutive framework for arterial wall mechanics and a comparative study of material models', *Journal of elasticity and the physical science of solids* **61**(1-3), 1–48.

Holzapfel, G. A., Sommer, G., Gasser, C. T. & Regitnig, P. (2005), 'Determination of layer-specific mechanical properties of human coronary arteries with nonatherosclerotic intimal thickening and related constitutive modeling', *American Journal of Physiology-Heart and Circulatory Physiology* **289**(5), H2048–H2058.

Iwaki, M., Wickham, S., Ikezaki, K., Yanagida, T. & Shih, W. (2016), 'A programmable dna origami nanospring that reveals force-induced adjacent binding of myosin vi heads', *Nature communications* **7**(1), 1–10.

Kelly-Arnold, A., Maldonado, N., Laudier, D., Aikawa, E., Cardoso, L. & Weinbaum, S. (2013), 'Revised microcalcification hypothesis for fibrous cap rupture in human coronary arteries', *Proceedings of the National Academy of Sciences* **110**(26), 10741–10746.

Korshunov, V. A. & Berk, B. C. (2004), 'Strain-dependent vascular remodeling: the Glagov phenomenon is genetically determined', *Circulation* **110**(2), 220–226.

Korshunov, V. A., Schwartz, S. M. & Berk, B. C. (2007), 'Vascular remodeling: hemodynamic and biochemical mechanisms underlying Glagovs phenomenon', *Arteriosclerosis, thrombosis, and vascular biology* **27**(8), 1722–1728.

Langille, B. L. (1996), 'Arterial remodeling: relation to hemodynamics', *Canadian journal of physiology and pharmacology* **74**(7), 834–841.

Langille, B. L. & O'Donnell, F. (1986), 'Reductions in arterial diameter produced by chronic decreases in blood flow are endothelium-dependent', *Science* **231**(4736), 405–407.

Langtangen, H. P., Logg, A. & Tveito, A. (2016), *Solving PDEs in Python: The FEniCS Tutorial I*, Springer International Publishing.

Libby, P., Ridker, P. M. & Maseri, A. (2002), 'Inflammation and atherosclerosis', *Circulation* **105**(9), 1135–1143.

Mohiaddin, R., Burman, E., Prasad, S., Varghese, A., Tan, R., Collins, S., Hughes, R., Gatehouse, P., Jhooti, P., Longmore, D. et al. (2004), 'Glagov remodeling of the atherosclerotic aorta demonstrated by cardiovascular magnetic resonance: the corda asymptomatic subject plaque assessment research (caspar) project', *Journal of Cardiovascular Magnetic Resonance* **6**(2), 517–525.

Mundi, S., Massaro, M., Scoditti, E., Carluccio, M. A., van Hinsbergh, V. W., Iruela-Arispe, M. L. & De Caterina, R. (2017), 'Endothelial permeability, ldl deposition, and cardiovascular risk factorsa review', *Cardiovascular research* **114**(1), 35–52.

Nakagawa, K. & Nakashima, Y. (2018), 'Pathologic intimal thickening in human atherosclerosis is formed by extracellular accumulation of plasma-derived lipids and dispersion of intimal smooth muscle cells', *Atherosclerosis* **274**, 235–242.

Rodriguez, E. K., Hoger, A. & McCulloch, A. D. (1994), 'Stress-dependent finite growth in soft elastic tissues', *Journal of biomechanics* **27**(4), 455–467.

Sanyal, A. & Han, H.-C. (2015), 'Artery buckling affects the mechanical stress in atherosclerotic plaques', *Biomedical engineering online* **14**(1), S4.

Schwartz, S. M., deBlois, D. & OBrien, E. R. (1995), 'The intima: soil for atherosclerosis and restenosis', *Circulation research* **77**(3), 445–465.

Sho, M., Sho, E., Singh, T. M., Komatsu, M., Sugita, A., Xu, C., Nanjo, H., Zarins, C. K. & Masuda, H. (2002), 'Subnormal shear stress-induced intimal thickening requires medial smooth muscle cell proliferation and migration', *Experimental and molecular pathology* **72**(2), 150–160.

Taber, L. A. & Humphrey, J. D. (2001), 'Stress-modulated growth, residual stress, and vascular heterogeneity', *Journal of biomechanical engineering* **123**(6), 528–535.

Tsai, W.-C., Wu, K.-Y., Lin, G.-M., Chen, S.-J., Lin, W.-S., Yang, S.-P., Cheng, S.-M. & Lin, C.-S. (2017), 'Clinical characteristics of patients less than forty years old with coronary artery disease in taiwan: a cross-sectional study', *Acta Cardiologica Sinica* **33**(3), 233.

Ueba, H., Kawakami, M. & Yaginuma, T. (1997), 'Shear stress as an inhibitor of vascular smooth muscle cell proliferation: role of transforming growth factor-β1 and tissue-type plasminogen activator', *Arteriosclerosis, thrombosis, and vascular biology* **17**(8), 1512–1516.

Virmani, R., Narula, J., Leon, M. B. & Willerson, J. T. (2008), *The vulnerable atherosclerotic plaque: strategies for diagnosis and management*, John Wiley & Sons.

Von Maltzahn, W.-W., Besdo, D. & Wiemer, W. (1981), 'Elastic properties of arteries: a nonlinear two-layer cylindrical model', *Journal of Biomechanics* **14**(6), 389–397.

Wayman, B. H., Taylor, W. R., Rachev, A. & Vito, R. P. (2008), 'Arteries respond to independent control of circumferential and shear stress in organ culture', *Annals of biomedical engineering* **36**(5), 673–684.

Yin, S.-F., Xue, S.-L., Li, B. & Feng, X.-Q. (2019), 'Bio–chemo–mechanical modeling of growing biological tissues: Finite element method', *International Journal of Non-Linear Mechanics* **108**, 46–54.

Zienkiewicz, O. C. & Taylor, R. L. (2005), *The finite element method for solid and structural mechanics*, Elsevier.